IJRCS

International Journal of Robotics and Control Systems
Vol. 4, No. 4, 2024, pp. 1731-1745
ISSN 2775-2658
http://pubs2.ascee.org/index.php/ijrcs

ASCEE

# Dynamic Assessment and Control of a Dual Star Induction Machine State Dedicated to an Electric Vehicle Under Short-Circuit Defect

Basma Benbouya [a,1], Hocine Cheghib [a,2], Meriem Behim [a,3], Mohamed Metwally Mahmoud [b,4], Mohamed F. Elnaggar [c,d,5,*], Nagwa F. Ibrahim [e,6], Noha Anwer [f,7]

[a] Laboratory of Electromechanical Systems, Department of Electromechanics, Faculty of Technology, Badji Mokhtar Annaba University, 23000, Annaba, Algeria
[b] Electrical Engineering Department, Faculty of Energy Engineering, Aswan University, Aswan 81528, Egypt
[c] Department of Electrical Engineering, College of Engineering, Prince Sattam Bin Abdulaziz University, Al-Kharj 11942, Saudi Arabia
[d] Department of Electrical Power and Machines Engineering, Faculty of Engineering, Helwan University, Helwan 11795, Egypt
[e] Electrical Department, Faculty of Technology and Education, Suez University, Suez 43533, Egypt
[f] Electrical Power and Machines Eng. Dept., The High Institute of Engineering and Technology, Luxor, Egypt
[1] basma.benbouya@univ-annaba.dz; [2] hocine.cheghib@univ-annaba.dz; [3] meriem.behim@univ-annaba.dz;
[4] Metwally_M@aswu.edu.eg; [5] mfelnaggar@yahoo.com; [6] nagwa.ibrahim@ind.suezuni.edu.eg;
[7] nohaanwer69@yahoo.com
* Corresponding Author

ARTICLE INFO

**Article history**
Received August 07, 2024
Revised September 09, 2024
Accepted October 14, 2024

**Keywords**
Dual Star Induction Machine;
Short-Circuit Defect;
Current Space Vector;
Wavelet Packet
Decomposition Energy;
Electric Vehicle

ABSTRACT

The widespread use of electric vehicles (EVs) in several industries gives rise to many significant safety and reliability-related issues. Thus, there is a need for methods for identifying flaws in EV components. In this paper, a state assessment of a dual star induction machine (DSIM) under short-circuit faults is investigated. The DSIM is selected due to its widespread use in high-power applications and its numerous advantages over other conventional machine types. Our focus is particularly on its application in the automotive industry, where its dual stator windings ensure reliable and robust parallel operation, thereby enhancing its robustness and efficiency. To improve this technology and ensure its proper functioning following potential failures and during maintenance, appropriate diagnostic and monitoring methods are essential. Our methodology combines two techniques: the current space vector (CSV), utilized to prevent information loss, and the wavelet packet decomposition energy, calculated from the resulting CSV signals. This approach enables the detection of various stator short-circuit faults, presenting different severities and occurring at different locations. The outcomes of this study, which were verified through the use of a Simulink model of a DSIM devoted to an EV, showcase the efficacy of the suggested approach. Furthermore, this work underscores the significance of this approach in maintaining the performance and reliability of DSIM, particularly in demanding environments such as the automotive industry.

## 1. Introduction

The technological landscape has witnessed the emergence of a specialized machine known as the dual star induction machine (DSIM) [1]-[3]. This machine, characterized by its multiphase design comprising two stator windings and one rotor winding, exhibits distinct operational features. The stator windings, arranged in two identical three-phase stars, are spatially offset from each other by an angle α, ensuring balanced electrical distribution. This configuration enables enhanced performance and operational versatility [4], [5].

Over the past four decades, the utilization of DSIMs has significantly surged across various high-power applications, notably in industries such as railways, petrochemicals, pumping stations, marine, aviation, aerospace, and particularly the automotive sector [6]-[8]. The adoption of DSIM stems from its inherent advantages over conventional multiphase machines, including reliability, robustness, efficiency, and exceptional performance compared to single-star configurations. Notably, DSIM mitigates electromagnetic torque ripples, curtails current harmonics, improves power factor, and facilitates half-speed operation. Moreover, its resilience in the face of phase failures or losses ensures continued operation, albeit in a degraded mode, minimizing torque fluctuations, segmenting power, enhancing efficiency, and exhibiting better tolerance to voltage and load imbalances [6]-[11].

Despite its merits, it is imperative to acknowledge the susceptibility of DSIM to faults, necessitating the implementation of appropriate diagnostic and monitoring methodologies to maintain operational integrity. However, the domain of DSIM fault diagnosis has received limited attention, given the complexity inherent in diagnosing defects in such machines. Existing fault diagnosis approaches in conventional IMs, as outlined in [12]-[17], underscore the intricate nature of fault detection, often requiring a combination of techniques for reliable results.

This underscores the need for further research in DSIM fault detection and diagnosis, particularly in the automotive sector, where high-power machines like DSIM play a critical role. Enhancing understanding of potential defects, reliability, and maintenance strategies tailored to DSIM is vital for optimizing efficiency and extending automobile operational life, especially in electric vehicles (EVs) [18]-[20].

Given the significance of short circuit defects as a major electrical fault in EVs, this study aims to develop a robust diagnostic method specifically tailored to DSIMs. Short circuit defects, encompassing turn-to-turn, coil-to-coil, phase-to-phase, and phase-to-ground faults, stem from various factors such as power imbalances, electrical overloads, stator core overheating, or rotor winding misalignment [21]-[24].

The proposed method integrates two techniques: current space vector (CSV) analysis and wavelet packet decomposition energy (WPDE) calculation, customized for DSIMs in EVs. Validation of this method is performed using a DSIM Simulink model, ensuring its applicability and accuracy in real-world applications.

## 2. Proposed Method Description

The methodology proposed in this paper consists of two main stages as seen in Fig. 1:

(a) Calculation of the CSV of the simulated six-phase current signals

Three sinusoidal waveforms, one for each phase of the system, show the currents in that system. These three quantities are combined into a single vector by the SV representation (eq. (1)), which offers a clear and effective means of expressing the state of the system [25], [26].

$$i(t) = \frac{1}{3}[i_1(t) + ai_2(t) + a^2 i_3(t)] \quad (1)$$

Where: a=e-j2/3π is the Fortescue operator.

(b) Calculation of the energy parameters for the approximations and WPD coefficients details,

The energy is an effective indicator for fault classification. According to [27], each frequency band's energy eigenvalue at a decomposition level j is defined as follows:

$$E_j = \sum_{n=1}^{N} \left| X_j(n) \right|^2 \tag{2}$$

Where: Xj(n) are the wavelet packet coefficients.

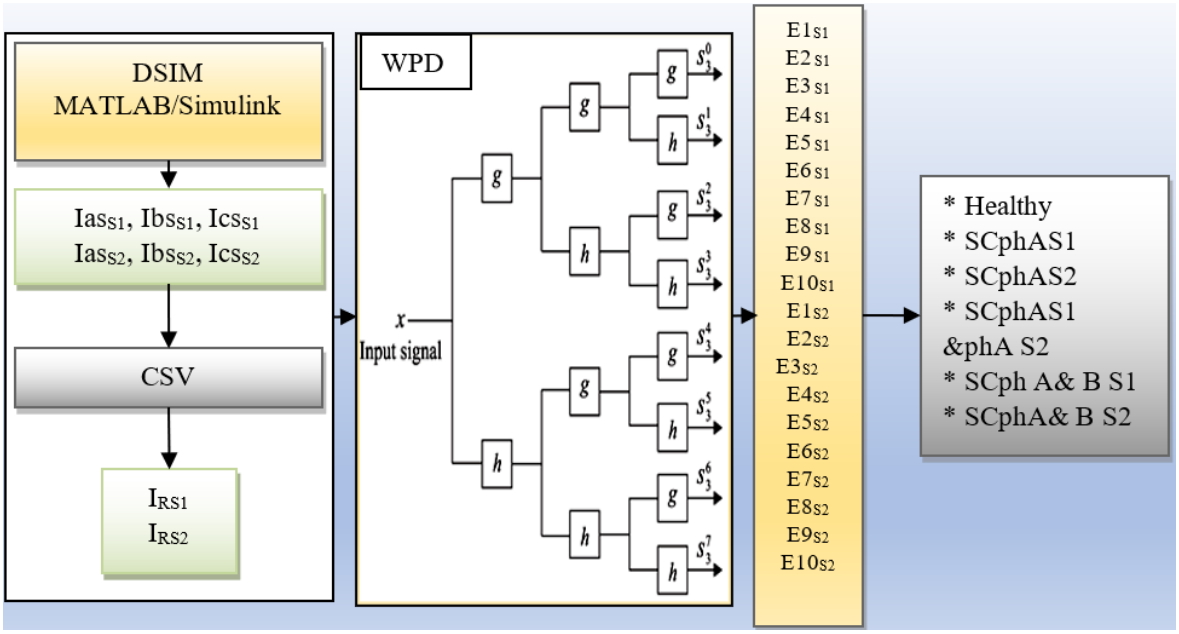


**Fig. 1.** Block diagram of the proposed new method

## 3. DSIM Model Including Short-Circuit Fault

The DSIM schematic shows the position of the winding axes of the nine phases that make up the machine as depicted in Fig. 2: six phases for the stator and three phases for the rotor. The mathematical representation of the DSIM linked to the "dq" axis system after applying the Park transformation to the stator voltages is expressed by equation (1) [28]-[30].

$$[B][\mathrm{U}] = [\mathrm{L}][i] - \omega_s[\mathrm{D}][\mathrm{I}] - \omega_{gl}[\mathrm{C}][\mathrm{I}] + [\mathrm{R}][\mathrm{I}] \tag{3}$$

$[U] = \left[v_{ds1}, v_{qs1}, v_{ds2}, v_{qs2}, v_{dr}, v_{qr}\right]^t$: Control vector

$[I] = \left[I_{ds1}, I_{qs1}, I_{ds2}, I_{qs2}, I_{dr}, I_{qr}\right]^t$ : State vector

$[i] = \left[i_{ds1}, i_{qs1}, i_{ds2}, i_{qs2}, i_{dr}, i_{qr}\right]$ : current vector

$[B] = diag[1\ 1\ 1\ 1\ 0\ 0]$

$[R] = diag\ [R_{s1} R_{s1} R_{s2} R_{s2} R_r R_r]$

$$[L] = \begin{bmatrix} (L_{s1}+L_m) & 0 & L_m & 0 & L_m & 0 \\ 0 & (L_{s1}+L_m) & 0 & L_m & 0 & L_m \\ L_m & 0 & (L_{s2}+L_m) & 0 & L_m & 0 \\ 0 & L_m & 0 & (L_{s2}+L_m) & 0 & L_m \\ L_m & 0 & L_m & 0 & (L_r+L_m) & 0 \\ 0 & L_m & 0 & L_m & 0 & (L_r+L_m) \end{bmatrix} \tag{4}$$

$$[D]=\begin{bmatrix} 0 & (L_{s1}+L_m) & 0 & L_m & 0 & L_m \\ -(L_{s1}+L_m) & 0 & -L_m & 0 & -L_m & 0 \\ 0 & L_m & 0 & (L_{s2}+L_m) & 0 & L_m \\ -L_m & 0 & -(L_{s2}+L_m) & 0 & -L_m & 0 \\ 0 & 0 & 0 & 0 & 0 & 0 \\ 0 & 0 & 0 & 0 & 0 & 0 \end{bmatrix} \quad (5)$$

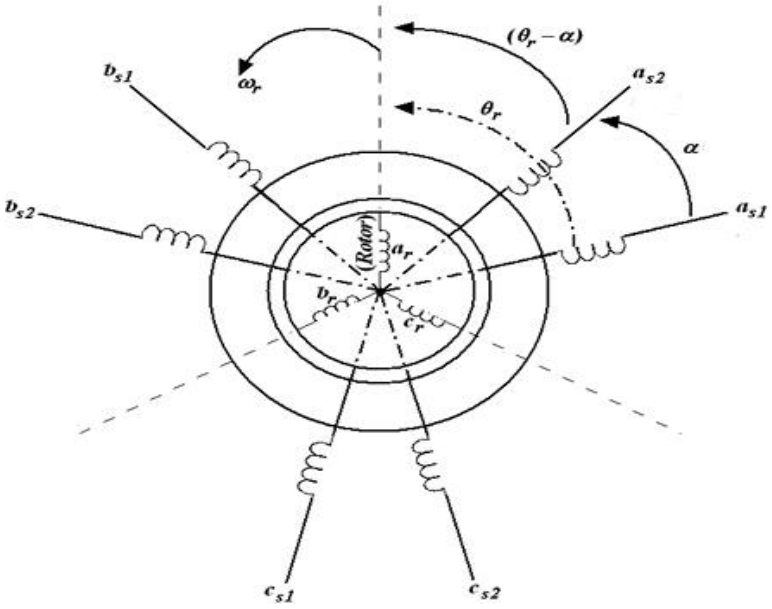


**Fig. 2.** Schematic representation of DSIM [31]

$$[C]=\begin{bmatrix} 0 & 0 & 0 & 0 & 0 & 0 \\ 0 & 0 & 0 & 0 & 0 & 0 \\ 0 & 0 & 0 & 0 & 0 & 0 \\ 0 & 0 & 0 & 0 & 0 & 0 \\ 0 & -L_m & 0 & L_m & 0 & (L_r+L_m) \\ -L_m & 0 & -L_m & 0 & -(L_r+L_m) & 0 \end{bmatrix} \quad (6)$$

For more details, voltage equations are:

$$Star\ 1:\begin{cases} v_{ds1}=R_{s1}i_{ds1}+\frac{d\varphi_{ds1}}{dt}-\omega_s\varphi_{qs1} \\ v_{qs1}=R_{s1}i_{qs1}+\frac{d\varphi_{qs1}}{dt}-\omega_s\varphi_{ds1} \end{cases} \quad (7)$$

$$Star\ 2:\begin{cases} v_{ds2}=R_{s2}i_{ds1}+\dfrac{d\varphi_{ds2}}{dt}-\omega_s\varphi_{qs2} \\ v_{qs2}=R_{s2}i_{qs2}+\dfrac{d\varphi_{qs2}}{dt}-\omega_s\varphi_{ds2} \end{cases} \quad (8)$$

$$Rotor:\begin{cases} v_{dr}=R_ri_{dr}+\dfrac{d\varphi_{dr}}{dt}-\omega_{gl}\varphi_{qr} \\ v_{qr}=R_ri_{qr}+\dfrac{d\varphi_{qr}}{dt}-\omega_{gl}\varphi_{dr} \end{cases} \quad (9)$$

And flux equations are represented as:

$$Star\ 1:\begin{cases} \varphi_{ds1}=L_{s1}i_{ds1}+L_m(i_{ds1}+i_{ds2}+i_{dr}) \\ \varphi_{qs1}=L_{s1}i_{qs1}+L_m(i_{qs1}+i_{qs2}+i_{qr}) \end{cases} \quad (10)$$

$$Star\ 2: \begin{cases} \varphi_{ds2} = L_{s2} i_{ds2} + L_m (i_{ds1} + i_{ds2} + i_{dr}) \\ \varphi_{qs2} = L_{s2} i_{qs2} + L_m (i_{qs1} + i_{qs2} + i_{qr}) \end{cases} \quad (11)$$

$$Rotor: \begin{cases} \varphi_{dr} = L_r i_{dr} + L_m (i_{ds1} + i_{ds2} + i_{dr}) \\ \varphi_{qr} = L_r i_{qr} + L_m (i_{qs1} + i_{qs2} + i_{qr}) \end{cases} \quad (12)$$

Based on the predefined mathematical expressions (1)-(10) a simulated model of a DSIM dedicated to an EV has been designed using the Simulink/MATLAB tool to diagnose all the resulting healthy and faulty signals as shown in Fig. 3. To simulate turn-to-turn short-circuit defects a set of modifications has been considered. In the case of turn-to-turn short-circuit in phase A, these modifications can be represented as follows [32], [33]:

$$In\ star\ 1: V_{abcs_1} = r_{s1} i_{abcs_1} + \frac{d\varphi_{abcs_1}}{dt} - \mu \begin{bmatrix} r_{s1} \\ 0 \\ 0 \end{bmatrix} i_f \quad (13)$$

$$In\ star\ 2: V_{abcs_2} = r_s i_{abcs_2} + \frac{d\varphi_{abcs_2}}{dt} - \mu \begin{bmatrix} r_{s2} \\ 0 \\ 0 \end{bmatrix} i_f \quad (14)$$

Where: if the short circuit current in phase A and μ is the defect percentage.

Applying Park transformation can be expressed as:

$$In\ star\ 1: V_{qd0_{s1}} = r_{s1} i_{qd0_{s1}} + \omega \varphi_{qd0_{s1}} + \frac{d\varphi_{qd0_{s1}}}{dt} - \sqrt{\frac{2}{3}} \mu r_{s1} \begin{bmatrix} \cos\theta \\ \sin\theta \\ 1/2 \end{bmatrix} i_f \quad (15)$$

$$In\ star\ 2: V_{qd0_{s2}} = r_{s2} i_{qd0_{s2}} + \omega \varphi_{qd0_{s2}} + \frac{d\varphi_{qd0_{s2}}}{dt} - \sqrt{\frac{2}{3}} \mu r_{s2} \begin{bmatrix} \cos\theta \\ \sin\theta \\ 1/2 \end{bmatrix} i_f \quad (16)$$

The parameters of the DSIM used for this study are summarized in Table 1.

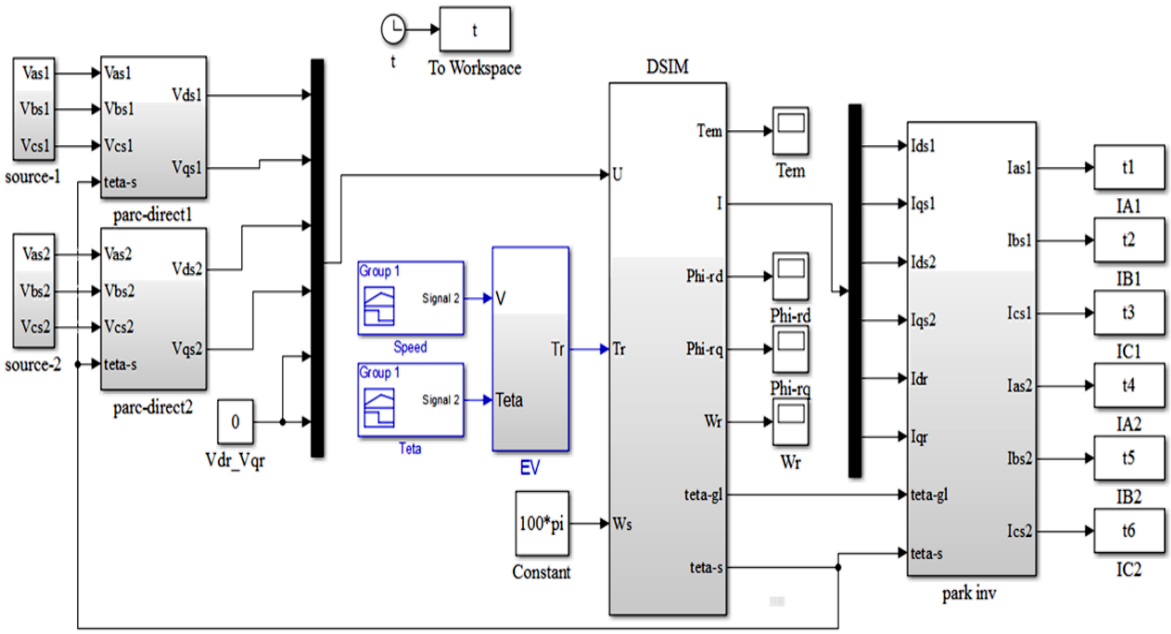


**Fig. 3.** Model of DSIM in the MATLAB/Simulink

**Table 1.** DSIM parameters

| Parameter | Value |
|---|---|
| Nominal power | $P_n$=100 kW |
| Nominal torque | $T_n$=650 N.m |
| Nominal voltage | $V_n$=220/380 V |
| Nominal current | $I_n$=90 A |
| Number of pole pairs | $p$=2 |
| Moment of inertia | $J$=2.5 kg m$^2$ |
| Coefficient of friction | $k_f$=0.04 Nms/rad |
| Rotor resistance | $R_r$ =0.021 Ω |
| Windingresistancestar 1 | $R_{s1}$=0.071 Ω |
| Windingresistancestar 2 | $R_{s2}$=0.071 Ω |
| Leakage inductances of star 1 windings | $L_{s1}$=0.0007 H |
| Leakage inductances of star 2 windings | $L_{s2}$=0.0007 H |
| Rotor inductance | $L_r$=0.000335 H |
| Cyclicmutual inductance | $L_m$= 0.0151 H |

## 4. Dimensional Study of the Charge

This study is based on the detection of short-circuit faults in the DSIM, which powers the EV as seen in Fig. 4. Therefore, the EV represents the charge. So, the various forces acting on the investigated EV are as follows:

$$Resistant\ force\ (\mathrm{F_{slope}}): F_{slope} = mg\sin(\beta) \tag{17}$$

$$Air\ penetration\ resistance\ force\ (\mathrm{F_{æro}}): F_{aero} = \frac{1}{2}\rho_{air}A_f C_d V_e^2 \tag{18}$$

$$Rolling\ resistance\ force\ (\mathrm{F_{tire}}): \quad F_{tire} = mgf_{ro}\cos(\beta) \tag{19}$$

$$The\ total\ resistive\ force\ is: F_r = F_{aero} + F_{tire} + F_{slope} \tag{20}$$

Introducing the system of equations (17), (18) and (19) in equation (20).

$$With, the\ equation\ of\ motion: m\frac{dV_{ev}}{dt} = F - F_r \tag{21}$$

We get:

$$The\ mechanical\ power\ of\ an\ EV\ is: \mathrm{P_{ev}} = \mathrm{F_r}.\mathrm{V_e} \tag{22}$$

$$The\ motor\ torque\ EV\ is: T_r = F_r\frac{r}{G} \tag{23}$$

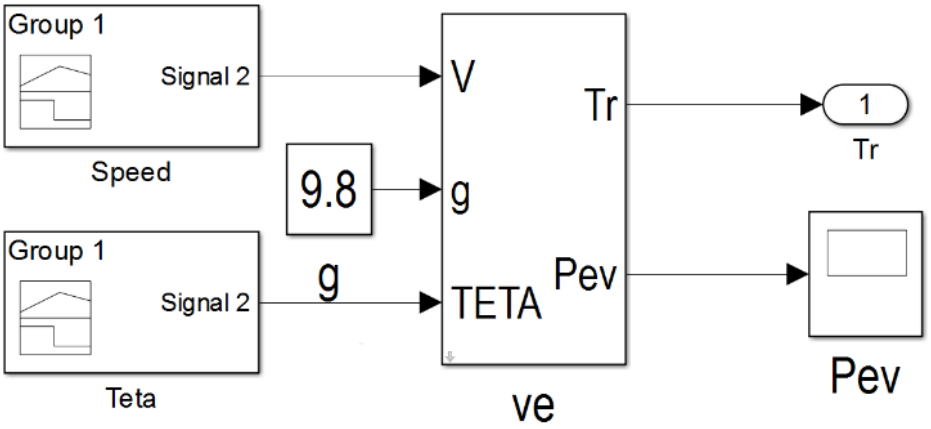


**Fig. 4.** Dimensional study of an EV in the MATLAB/Simulink

## 5. Results and Discussion

For this study, six cases of defects, starting at t=1s, are considered: healthy DSIM, short-circuit in phase *A* star1, short-circuit in phase *A* star2, short-circuit in phase *A* star1 and phase *A* star2, phase *A* and *B* star1, phase *A* and *B* star2; under several severities (30%, 40%, and 50%); in three cases, an EV without load, with a speed variation between (50 km/h) and (100 km/h) with no slope, and a slope variation of (30°) and (-30°) with a fixed speed of 80 km/h.

### 5.1. Simulated Data Acquisition

The signals are obtained by MATLAB/Simulink software with a sampling frequency of 1000 Hz.

#### 5.1.1. EV Motor Without Load

Fig. 5 represents the module of CSV of simulated signals for the two stars in the healthy and faulty state in case phases *A* and *B* turn to short-circuit of the first star with no load.

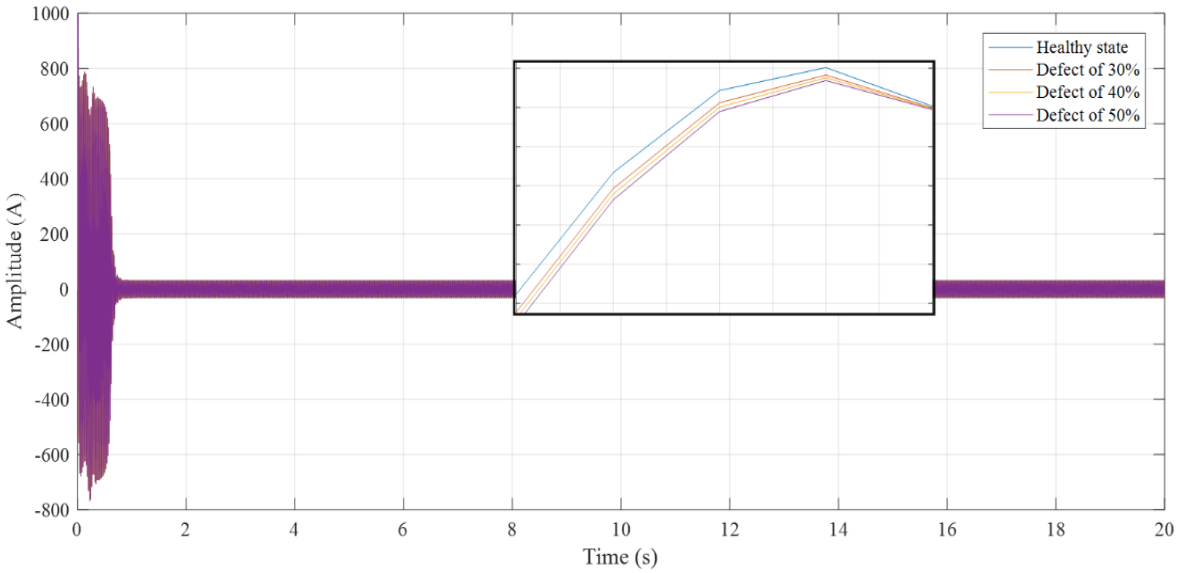


**Fig. 5.** CSV module of simulated signals in the healthy and faulty state with no load

#### 5.1.2. EV Motor With a Speed Variation

Fig. 6 represents the module of CSV of simulated signals for the two stars in the healthy and faulty state in case of phases and *B* turn to turn to short-circuit of the first star with speed variation and no slope.

#### 5.1.3. EV Motor With a Slope Variation

Fig. 7 represents the module of CSV of simulated signals for the two stars in the healthy and faulty state in case of phases and *B* turn to turn to short-circuit of the first star with slope variation and fixed speed at 80km/h.

### 5.2. 5.2 Data Decomposition

To treat the state of the DSIM, the trasatory part of the signal was eliminated and only its stationary part was considered for the treatment. The WPD of the CSV signal is done with Daubchies 'db44' mother wavelet and the decomposition level is calculated by the relation [34], [35]:

$$N=\text{int}\left(\frac{\log\left({}^{f_s}/_{f_e}\right)}{\log(2)}\right)+2 \quad (24)$$

With: $f_s$: sampling frequency ($f_s$=10000 Hz), fe: supply frequency ($f_e$=50 Hz), and so N=9.

### 5.2.1. EV Motor Without Load

Fig. 8 represents the energy values corresponding to the ninth-level WPD nodes for healthy and defective states under severity of 50% for each case, for both star 1 and star 2, with no applied load. These results make differences between the healthy state and the several studied defects; where, it is outstanding that the energy values in star 2 are more important in comparison to star 1 due to the phase shift between the two stars; we can notice also, that the highest energy value corresponds to the defects related to the star where the defect is occurring and vice versa as explained in Table 2. It also appeared that the energy concentration is around the 5$^{th}$ node so we have selected and compared the energies of this node for the rest of the tests.

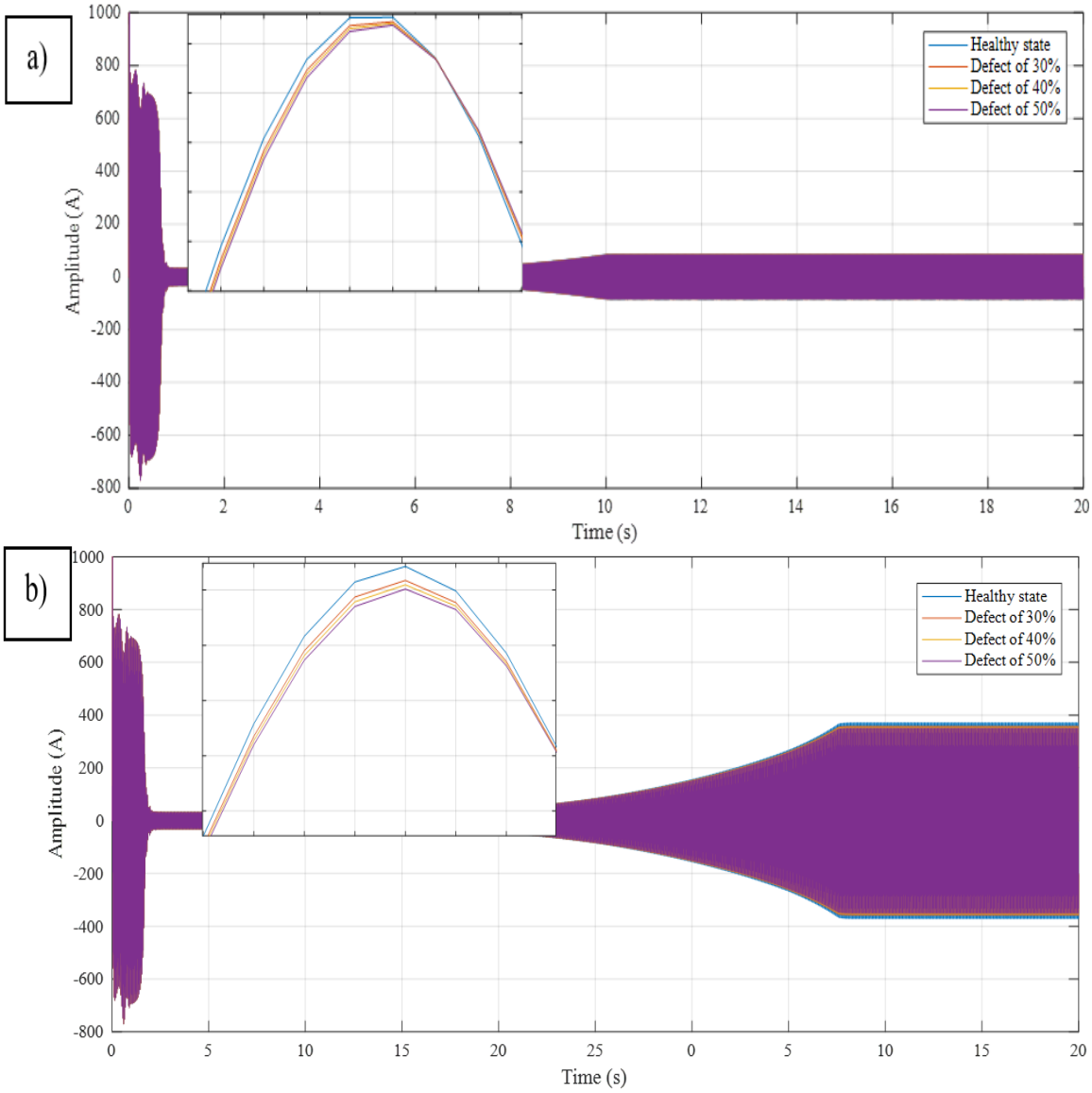


**Fig. 6.** CSV module of simulated signals in the healthy faulty state under speed variation: a)50 km/h, b)100 Km/h

**Table 2.** Ascending order of energy values

| | Lowest Energy Values | | | Highest Energy Values | | |
|---|---|---|---|---|---|---|
| **Star 1** | Phase A S2 | Phase A and B S2 | Phase A S1 and S2 | Healthy | Phase A and B S1 | Phase A S1 |
| **Star 2** | Phase A S1 | Phase A and B S1 | Phase A S1 and S2 | Healthy | Phase A and B S2 | Phase A S2 |

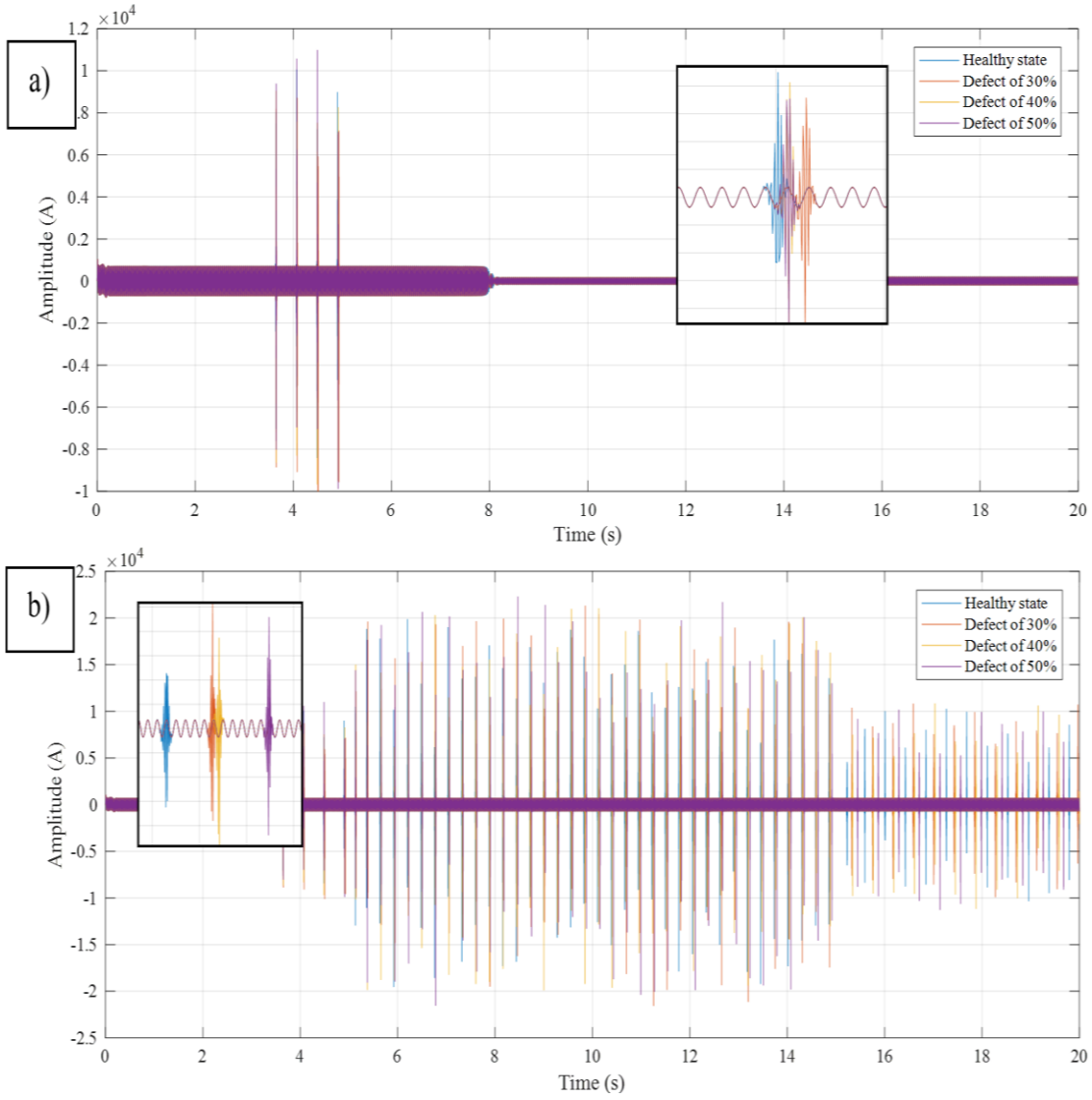


**Fig. 7.** CSV module of simulated signals in the healthy faulty state under slope variation: a) -30°, b) 30°

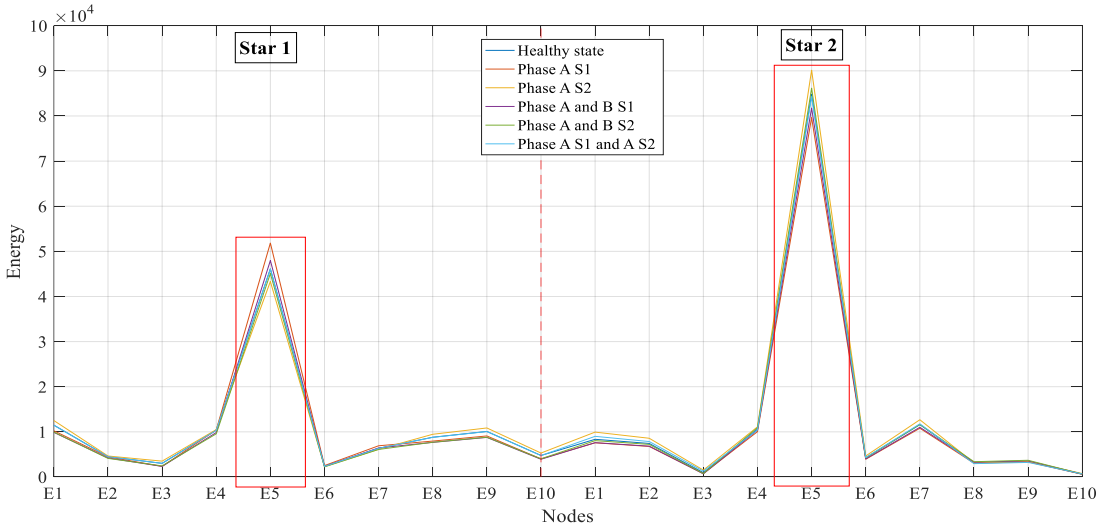


**Fig. 8.** Energy values of the WPD nodes: without load

### 5.2.2. EV Motor With a Speed Variation

Fig. 9 and Fig. 10 represent the energy values corresponding to the fifth node of the ninth-level WPD for the several obtained defect types at the different considered severities of 30%, 40%, and 50% of damage. Besides the remarks obtained from the first tests (part a), we can see that the energy values increase with the increase of damage severity for the defects from the same star and decrease for the defects from the opposite one when applying a speed of 50 km/h (low load) and vice versa when applying a speed variation of 100 km/h (high load). Besides the influence of speed variation, where the energy of the two stars becomes almost homogeneous when applying a speed of 100 km/h; also, the energy values for the speed of 100 km/h represent nearly twice the value of those of 50 km/h of speed.

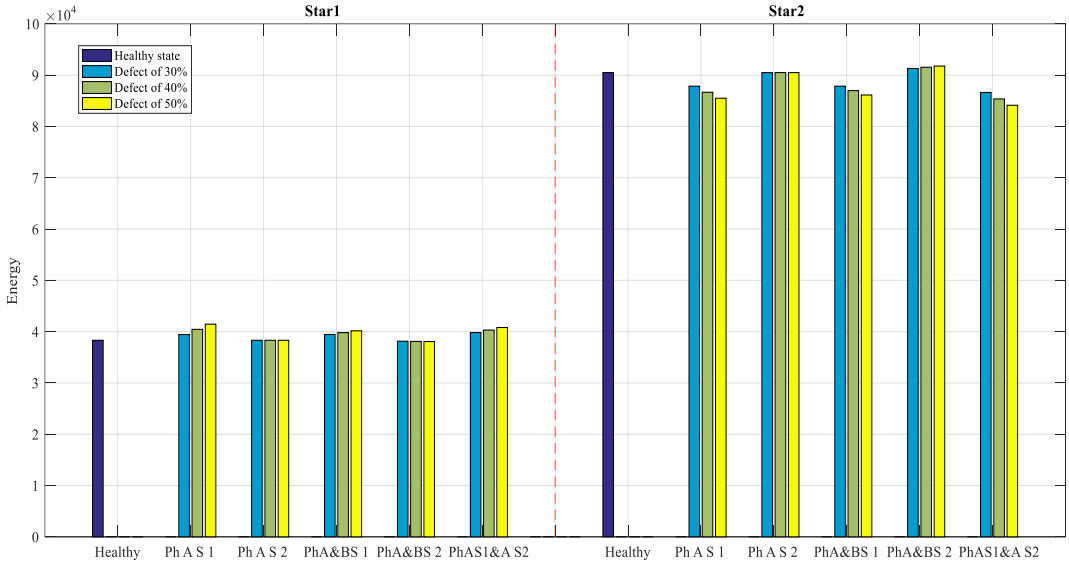


**Fig. 9.** Energy values corresponding to the fifth node of the ninth-level WPD: speed variation (50 km/h)

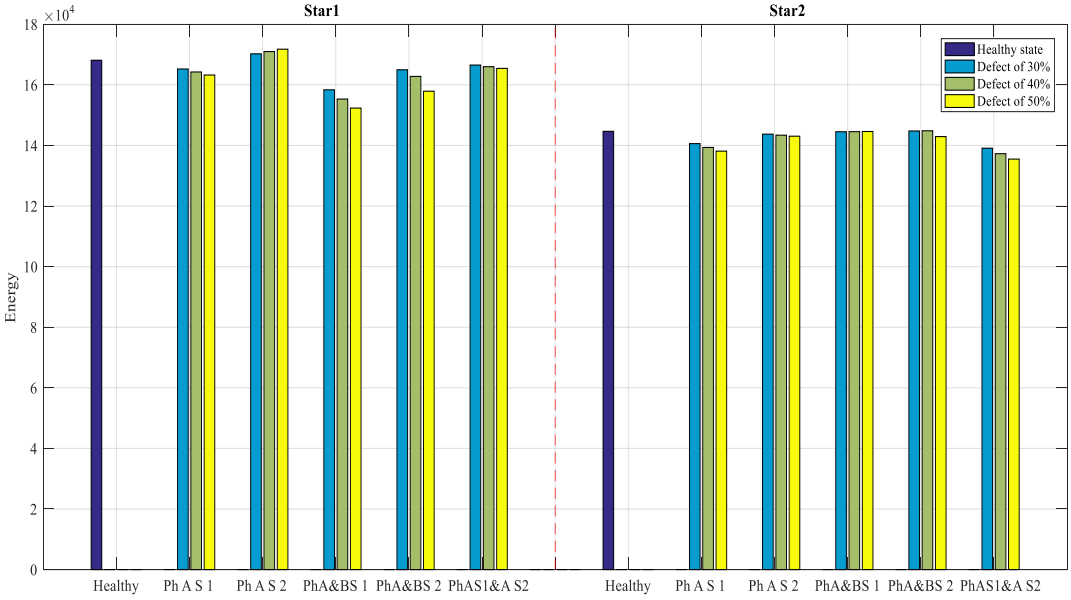


**Fig. 10.** Energy values corresponding to the fifth node of the ninth-level WPD: speed variation (100 km/h)

### 5.2.3. EV Motor With a Slope Variation

Fig. 11 and Fig. 12 represent the energy values corresponding to the fifth node of the ninth-level WPD for the several obtained defect types at the different considered severities of 30%, 40%, and

50% of damage. We can note that the energies for both slopes of (30°) and (-30°) behave in the same way as those at 50 km/h, however, it takes the highest values when comparing with tests without load and with speed variations. To evaluate the efficacy of the suggested approach, Table 3 offers a comparison with other research on inter-turn short circuit fault diagnosis of EV motors.

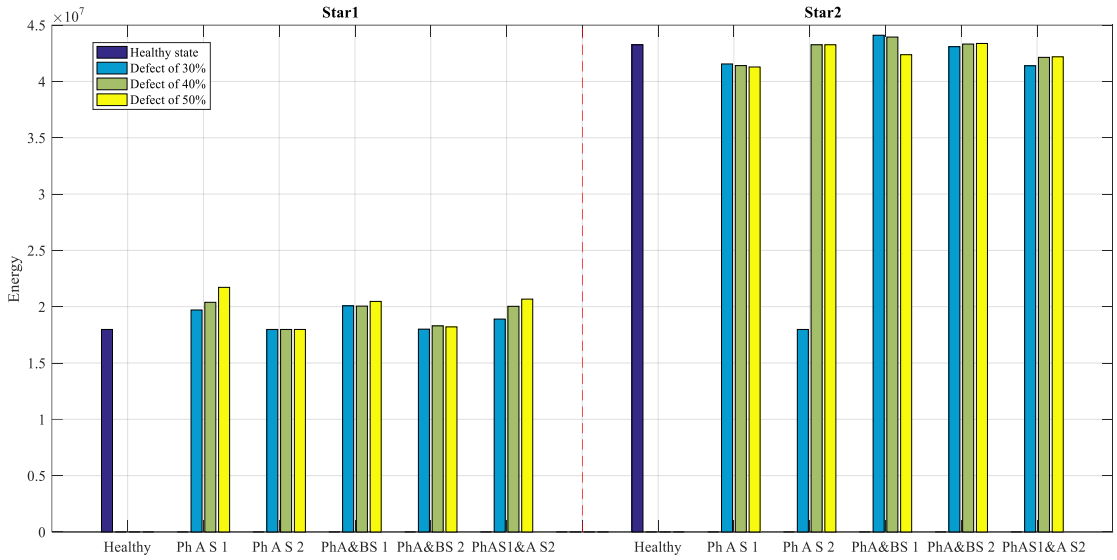


**Fig. 11.** Energy values corresponding to the fifth node of the ninth-level WPD: slope variation (30°)

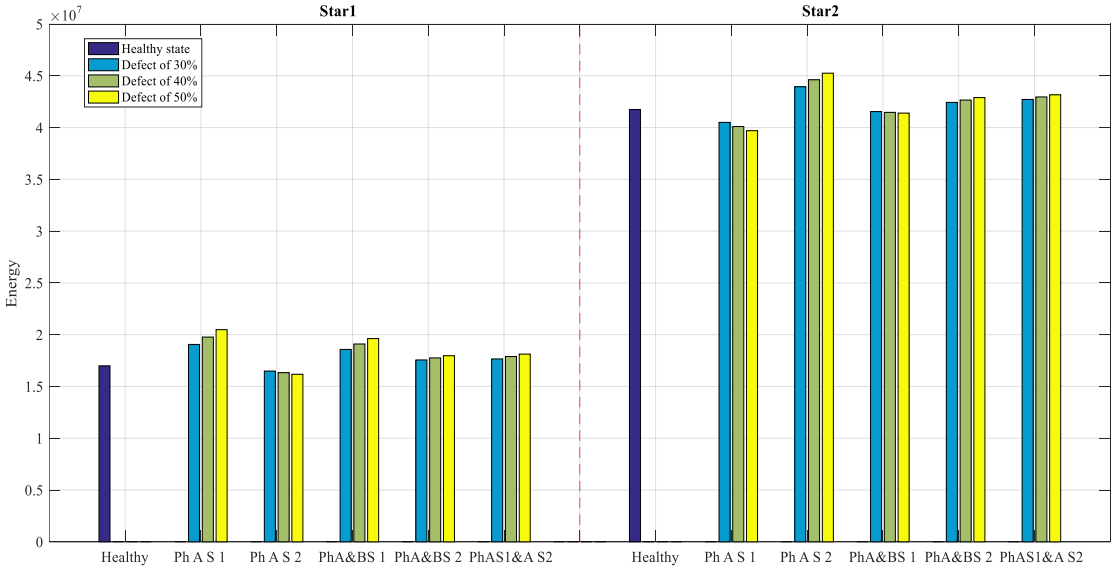


**Fig. 12.** Energy values corresponding to the fifth node of the ninth-level WPD: slope variation (-30°)

**Table 3.** Comparative analysis of EV motors' ITSC fault detection.

| Reference | Motor type | Method | Remarks |
|---|---|---|---|
| [36] | permanent magnetic synchronous motor (PMSM) | Deep Reinforcement Learning | Accuracy of 99.99%. |
| [37] | PMSM | Combination of Park's vector + Multimodal mobile net v2 | Accuracy of 99.26%. |
| [38] | PMSM | Fuzzy-Extended Kalman Filter | High precision in detecting the defects with a medium complexity of the proposed method application. |
| Present paper | DSIM | Current space vector and WPD Energy | A good indication of defects under different speed and slope conditions. |

## 6. Conclusions

The DSIM is a powerful machine with a reduced possibility of degradation compared to other IMs, it is chosen for its reliability and its ability to continue the service in case of partial electrical failures so it is used in this research for the motorization of an EV. In this paper, we have dealt with inter-turn short circuit fault which represents the most relevant fault that occurs in IMs. A simple and efficient approach was introduced in this paper for early detection and diagnosis of a stator short-circuit defect in a DSIM using WPDE enhanced by CSV technique. The proposed method is evaluated using simulated stator short-circuit defects obtained by MATLAB/Simulink environment under several severities with variations of speed and slope. Switching the presented results, we can conclude a set of important points:

- With a low load, the energy values of the second star are higher than the first star due to the phase shift between the two stars.
- The highest energy value corresponds to the defects related to the star where the defect is occurring.
- The energy values decrease with the increase of defect severity when the defect is considered a minor defect with a minor load.
- The energy values increase with the increase of defect severity when the defect is considered a minor defect with the major load.
- The defects appear more clearly when changing slope than speed because EVs in the first case need more power to move compared to a road without slope.

**Author Contribution:** All authors contributed equally to the main contributor to this paper. All authors read and approved the final paper.

**Data Availability:** The data used to support the findings of this study are available at reasonable request from the corresponding author.

**Acknowledgment:** This study is supported via funding from Prince sattam bin Abdulaziz University project number (PSAU/2024/R/1446).

**Conflicts of Interest:** The authors declare that they have no conflicts of interest.

### List of Abbreviations and Notations

DSIM: Dual star induction machine
$V_{a, b, c1}$: Three-phase voltages of star 1
$V_{a, b, c2}$: Three-phase voltages of star 2
$V_{a, b, c}$: Three-phase voltages of the rotor
$V_{d, q, s1}$: Voltages of star 1 in Park reference frame “d, q”
$Vd, q, s2$: Voltages of star 2 in Park reference frame “d, q “
$Vd, q, r$: Rotor voltages in Park reference frame “d, q “
$Ia_{, b, c1}$: Three-phase currents of star 1
$Ia_{, b, c2}$: Three-phase currents of star 2
$Ia_{,b,cr}$: Three-phase currents of the rotor
$id,q,s1$: Star 1 currents in the Park reference frame “d, q”
$id,qs2$: Star 2 currents in Park reference frame “d, q”
$id,qr$: Rotor currents in Park reference frame “d, q”
$\varphi d,qs1$: Flux of star 1 in Park reference frame “d, q”
$\varphi d,qs2$: Flux of star 2 in Park reference frame “d, q “
$\varphi d,qr$: Rotor fluxes in the Park reference frame “d, q “
$Rs1$: Resistances of the first star phases
$Rs2$: Resistances of the second star phases

$Rr$; Resistance of the rotor
$Lm$: Cyclic mutual inductance between star 1 and star 2
$Lr$ Rotor inductance
$Ls1$: Stator inductance of star 1
$Ls2$: Stator inductance of star 2
$\omega_s$: Fundamental electrical pulse of the stator magnitudes
$\omega_{gl}$: Fundamental electric pulse of the slip
g The gravity
β: The slope angle of the road
$\boldsymbol{r}$: Wheel radius
G: Speed reducer
$J$: Total inertia of rotating parts
p: Number of pole pairs
$g$: Slip
$F$: Network Frequency
$K$: Stator-rotor magnetic coupling coefficient
$\varphi f$: Flux imposed by the excitation current $if$
$f_{ro}$: The constant of the resistance force due to the displacement
$\rho_{air}$: The density of the air
$A_f$: The frontal area of the vehicle
$C_d$: The aerodynamic drag coefficient;
G: Speed reducer gain of the electric vehicle
m: The total mass of the vehicle
$V_{ev}$: The speed of the vehicle
$P_{ev}$: The power of the electric vehicle
$F_r$ : The total resistive force

## References

[1] H. Lallouani and B. Saad, "Performances of type 2 fuzzy logic control based on direct torque control for double star induction machine," *Revue Roumaine des Sciences Techniques, Série Électrotechnique et Énergétique*, vol. 65, no. 1-2, pp. 103-108, 2020, http://www.revue.elth.pub.ro/upload/54433318_HLallouani_RRST_1-2_2020_pp_103-108.pdf.

[2] M. Chebaani, M. M. Mahmoud, A. F. Tazay, M. I. Mosaad, and N. A. Nouraldin, "Extended Kalman Filter design for sensorless sliding mode predictive control of induction motors without weighting factor: An experimental investigation," *PLoS One*, vol. 18, no. 11, p. e0293278, 2023, https://doi.org/10.1371/journal.pone.0293278.

[3] M. Nesri, H. Benkadi, K. Nounou, G. Sifelislam, and M. F. Benkhoris, "Fault Tolerant Control of a Dual Star Induction Machine Drive System using Hybrid Fractional Controller," *Power Electronics and Drives*, vol. 9, no. 1, pp. 161-175, 2024, https://doi.org/10.2478/pead-2024-0010.

[4] K. Hamitouche, S. Chekkal, H. Amimeur, and D. Aouzellag, "A new control strategy of dual stator induction generator with power regulation," *Journal Européen des Systèmes Automatisés*, vol. 53, no. 4, pp. 469-478, 2020, https://doi.org/10.18280/jesa.530404.

[5] S. Verma, A. Kumar, and A. K. Gupta, "An Assessment and Performance of Voltage Source Inverter Feed Induction Motor Drive," *International Journal for Research in Applied Science & Engineering Technology*, vol. 12, no. 1, pp. 1306-1310, 2024, https://doi.org/10.22214/ijraset.2024.58151.

[6] N. Layadi, S. Zeghlache, T. Benslimane, and F. Berrabah, "Comparative analysis between the rotor flux oriented control and backstepping control of a double star induction machine (DSIM) under open-phase fault," *Advances in Modelling and Analysis C*, vol. 72, no. 4, pp. 292-311, 2017, https://doi.org/10.18280/ama_c.720407.

[7] F. Hamidia, A. Abbadi, A. Tlemçani, and M. S. Boucherit, "Dual star induction motor supplied with double photovoltaic panels based on fuzzy logic type-2," *Nonlinear Dynamics and Systems Theory*, vol. 18, no. 4, pp. 359-371, 2018, https://www.e-ndst.kiev.ua/v18n4/V18N4.pdf#page=45.

[8] N. F. Ibrahim, A. Alkuhayli, A. Beroual, U. Khaled, and M. M. Mahmoud, "Enhancing the Functionality

of a Grid-Connected Photovoltaic System in a Distant Egyptian Region Using an Optimized Dynamic Voltage Restorer: Application of Artificial Rabbits Optimization," *Sensors*, vol. 23, no. 16, p. 7146, 2023, https://doi.org/10.3390/s23167146.

[9] K. Iffouzar, M. F. Benkhoris, B. Amrouche, A. Houari, K. Ghedamsi, and A. Djerioui, "A New Post-Fault Reconfiguration Strategy under Open-Phase Operation Conditions of Asymmetrical Double-Star Induction Machines," *Energies*, vol. 16, no. 15, p. 5740, 2023, https://doi.org/10.3390/en16155740.

[10] H. Boudjemai *et al*., "Application of a Novel Synergetic Control for Optimal Power Extraction of a Small-Scale Wind Generation System with Variable Loads and Wind Speeds," *Symmetry*, vol. 15, no. 2, p. 369, 2023, https://doi.org/10.3390/sym15020369.

[11] I. E. Maysse *et al*., "Nonlinear Observer-Based Controller Design for VSC-Based HVDC Transmission Systems Under Uncertainties," *IEEE Access*, vol. 11, pp. 124014-124030, 2023, https://doi.org/10.1109/ACCESS.2023.3330440.

[12] J. J. Cardenas-Cornejo, M. A. Ibarra-Manzano, A. González-Parada, R. Castro-Sanchez, and D. L. Almanza-Ojeda, "Classification of inter-turn short-circuit faults in induction motors based on quaternion analysis," *Measurement*, vol. 222, p. 113680, 2023, https://doi.org/10.1016/j.measurement.2023.113680.

[13] M. Skowron, T. Orlowska-Kowalska, M. Wolkiewicz, and C. T. Kowalski, "Convolutional neural network-based stator current data-driven incipient stator fault diagnosis of inverter-fed induction motor," *Energies*, vol. 13, no. 6, p. 1475, 2020, https://doi.org/10.3390/en13061475.

[14] F. Javier Villalobos-Pina, J. Augusto Reyes-Malanche, E. Cabal-Yepez, and E. Ramirez-Velasco, "Electric Fault Diagnosis in induction Machines using Motor Current Signature Analysis (MCSA)," *Time Series Analysis - Recent Advances, New Perspectives and Applications*, 2024, https://doi.org/10.5772/intechopen.1004002.

[15] S. H. Ebrahimi, M. Choux, and V. K. Huynh, "Real-Time Detection of Incipient Inter-Turn Short Circuit and Sensor Faults in Permanent Magnet Synchronous Motor Drives Based on Generalized Likelihood Ratio Test and Structural Analysis," *Sensors*, vol. 22, no. 9, p. 3407, 2022, https://doi.org/10.3390/s22093407.

[16] J. A. Reyes-Malanche, F. J. Villalobos-Pina, E. Ramırez-Velasco, E. Cabal-Yepez, G. Hernandez-Gomez, and M. Lopez-Ramirez, "Short-Circuit Fault Diagnosis on Induction Motors through Electric Current Phasor Analysis and Fuzzy Logic," *Energies*, vol. 16, no. 1, p. 516, 2023, https://doi.org/10.3390/en16010516.

[17] A. Almounajjed, A. K. Sahoo, M. K. Kumar and S. K. Subudhi, "Stator Fault Diagnosis of Induction Motor Based on Discrete Wavelet Analysis and Neural Network Technique," *Chinese Journal of Electrical Engineering*, vol. 9, no. 1, pp. 142-157, 2023, https://doi.org/10.23919/CJEE.2023.000003.

[18] N. F. Ibrahim *et al*., "A new adaptive MPPT technique using an improved INC algorithm supported by fuzzy self-tuning controller for a grid-linked photovoltaic system," *PLoS One*, vol. 18, no. 11, p. e0293613, 2023, https://doi.org/10.1371/journal.pone.0293613.

[19] O. M. Kamel, A. A. Z. Diab, M. M. Mahmoud, A. S. Al-Sumaiti, and H. M. Sultan, "Performance Enhancement of an Islanded Microgrid with the Support of Electrical Vehicle and STATCOM Systems," *Energies*, vol. 16, no. 4, p. 1577, 2023, https://doi.org/10.3390/en16041577.

[20] S. R. K. Joga *et al*., "Applications of tunable-Q factor wavelet transform and AdaBoost classier for identification of high impedance faults: Towards the reliability of electrical distribution systems," *Energy Exploration & Exploitation*, 2024, https://doi.org/10.1177/01445987241260949.

[21] Y. Liu and A. M. Bazzi, "A review and comparison of fault detection and diagnosis methods for squirrel-cage induction motors: State of the art," *ISA Transactions*, vol. 70, pp. 400-409, 2017, https://doi.org/10.1016/j.isatra.2017.06.001.

[22] M. M. Mahmoud, "Improved current control loops in wind side converter with the support of wild horse optimizer for enhancing the dynamic performance of PMSG-based wind generation system," *International Journal of Modelling and Simulation*, vol. 43, no. 6, pp. 952-966, 2023, https://doi.org/10.1080/02286203.2022.2139128.

[23] M. Nesri, K. Nounou, G. Sifelislam, M. F. Benkhoris, and H. Azeddine, "Hybrid Flatness-Based Control

of Dual Star Induction Machine Drive System for More Electrical Aircraft," *Power Electronics and Drives*, vol. 9, no. 1, pp. 50-62, 2024, https://doi.org/10.2478/pead-2024-0004.

[24] N. Benalia *et al*., "Enhancing electric vehicle charging performance through series-series topology resonance-coupled wireless power transfer," *PLoS One*, vol. 19, no. 3, p. e0300550, 2024, https://doi.org/10.1371/journal.pone.0300550.

[25] M. Khalid Ratib *et al*., "Applications of hybrid model predictive control with computational burden reduction for electric drives fed by 3-phase inverter," *Ain Shams Engineering Journal*, vol. 14, no. 8, p. 102028, 2022, https://doi.org/10.1016/j.asej.2022.102028.

[26] H. Miloudi *et al*., "Electromagnetic Compatibility Characterization of Start-Capacitor Single-Phase Induction Motor," *IEEE Access*, vol. 12, pp. 2313-2326, 2024, https://doi.org/10.1109/ACCESS.2023.3349018.

[27] N. Lahouasnia, M. F. Rachedi, D. Drici, and S. Saad, "Load Unbalance Detection Improvement in Three-Phase Induction Machine Based on Current Space Vector Analysis," *Journal of Electrical Engineering & Technology*, vol. 15, pp. 1205-1216, 2020, https://doi.org/10.1007/s42835-020-00403-y.

[28] Z. Tir, Y. Soufi, M. N. Hashemnia, O. P. Malik, and K. Marouani, "Fuzzy logic field oriented control of double star induction motor drive," *Electrical Engineering*, vol. 99, no. 2, pp. 495-503, 2017, https://doi.org/10.1007/s00202-016-0377-2.

[29] F. Bu, Y. Hu, W. Huang, S. Zhuang and K. Shi, "Control Strategy and Dynamic Performance of Dual Stator-Winding Induction Generator Variable Frequency AC Generating System With Inductive and Capacitive Loads," *IEEE Transactions on Power Electronics*, vol. 29, no. 4, pp. 1681-1692, 2014, https://doi.org/10.1109/TPEL.2013.2265099.

[30] A. T. Hassan *et al*., "Adaptive Load Frequency Control in Microgrids Considering PV Sources and EVs Impacts: Applications of Hybrid Sine Cosine Optimizer and Balloon Effect Identifier Algorithms," *International Journal of Robotics and Control Systems*, vol. 4, no. 2, pp. 941-957, 2024, https://doi.org/10.31763/ijrcs.v4i2.1448.

[31] K. Marouani, F. Khoucha, A. Kheloui, L. Baghli and D. Hadiouche, "Study and Simulation of Direct Torque Control of Double-Star Induction Motor Drive," *2006 12th International Power Electronics and Motion Control Conference*, pp. 1233-1238, 2006, https://doi.org/10.1109/EPEPEMC.2006.4778571.

[32] C. F. d. Costa, M. A. Rocha, W. G. d. Souza, P. T. Justino and A. L. Andreoli, "Implementation of an Induction Motor Mathematical Model for Stator Winding Fault Analysis," *2018 13th IEEE International Conference on Industry Applications (INDUSCON)*, pp. 738-743, 2018, https://doi.org/10.1109/INDUSCON.2018.8627194.

[33] O. M. Lamine *et al*., "A Combination of INC and Fuzzy Logic-Based Variable Step Size for Enhancing MPPT of PV Systems," *International Journal of Robotics and Control Systems*, vol. 4, no. 2, pp. 877-892, 2024, https://doi.org/10.31763/ijrcs.v4i2.1428.

[34] Y. Wei, Y. Li, M. Xu, W. Huang, "A Review of Early Fault Diagnosis Approaches and Their Applications in Rotating Machinery," *Entropy*, vol. 21, no. 4, p. 409, 2019, https://doi.org/10.3390/e21040409.

[35] M. Behim, L. Merabet and S. Saad, "Diagnosis of Supply Voltage Imbalance Using WPD Energy Enhanced by Current Space Vector (CSV)," *2022 19th International Multi-Conference on Systems, Signals & Devices (SSD)*, pp. 242-245, 2022, https://doi.org/10.1109/SSD54932.2022.9955936.

[36] M. Mahfooth and O. Mahmood, "Detection and Diagnosis of Inter-Turn Short Circuit Faults of PMSM for Electric Vehicles Based on Deep Reinforcement Learning," *Al-Rafidain Engineering Journal*, vol. 28, no. 2, pp. 75-85, 2023, https://doi.org/10.33899/rengj.2023.138195.1229.

[37] Á. Zsuga and A. Dineva, "Data-Driven Onboard Inter-Turn Short Circuit Fault Diagnosis for Electric Vehicles by Using Real-Time Simulation Environment," *IEEE Access*, vol. 11, pp. 145447-145466, 2023, https://doi.org/10.1109/ACCESS.2023.3344483.

[38] M. Romdhane, M. Naoui, and A. Mansouri, "PMSM Inter-Turn Short Circuit Fault Detection Using the Fuzzy-Extended Kalman Filter in Electric Vehicles," *Electronics*, vol. 12, no. 18, p. 3758, 2023, https://doi.org/10.3390/electronics12183758.